J. Fluid Mech. (1982), *vol.* 114, *pp.* 399-418
Printed in Great Britain

Supercritical flow past symmetrical airfoils

By KON-MING LI AND MAURICE HOLT
Department of Mechanical Engineering, University of California, Berkeley, California

(Received 3 March 1981)

A numerical method is developed for computing steady supercritical flow about an ellipse at zero angle of attack. The flow is assumed to be two-dimensional, inviscid, isentropic and irrotational. The free-stream Mach number lies in the high subsonic range so that a shock wave occurs locally near the body. The full potential equations are solved by Telenin's method and the 'method of lines'. Smooth interpolating functions are assumed for the unknown flow variables in selected co-ordinate directions. The resulting set of ordinary differential equations is then integrated away from or along the body depending upon whether the flow is smooth or discontinuous. Jump conditions of the governing equations are applied across the shock wave so that it is perfectly sharp. A doublet solution for flow past a closed body is used as the far-field boundary condition. Supercritical flow calculations have been performed for ellipses with thickness ratio of 0·2 and 0·4 at various free-stream Mach numbers. The present results are compared with the shock-capturing method, and good agreement is obtained.

1. Introduction

Within the past decade there has been strong interest in transonic flow research. The fact that commercial jets often fly at transonic speeds makes it very desirable to have methods which can predict airfoil lift and drag in this flow regime.

The flow is called transonic if both subsonic and supersonic regions are present in the field. Although most airplanes fly at subsonic speeds, the local flow velocities often become supersonic at the top of the wing. In a typical transonic flow field, the embedded supersonic region is usually terminated by means of a shock wave.

The main difficulties in transonic flow calculations are due to the inherent non-linearities of the equations governing transonic flow, and the fact that the equations change type within the solution domain, from elliptic in the subsonic region to hyperbolic in the supersonic region. In addition, special provision must be made to handle the embedded shock wave in the flow field.

There are three main categories of numerical methods for solving steady inviscid flow past an airfoil in the transonic regime. These are finite-difference methods, the hodograph method and interpolation methods.

Finite-difference techniques have received the most attention in transonic flow research in recent years and we now outline them briefly.

Magnus & Yoshihara (1970) first solved the unsteady Euler equations using an explicit second-order difference scheme. Unfortunately, the method requires a very large amount of computation time to achieve steady-state conditions, and is therefore very expensive for practical calculations.

An alternative to the time-dependent approach is the use of relaxation methods. Murman & Cole (1971) successfully solved the transonic small-disturbance equations by introducing a mixed finite-difference system. The direction of differencing is biased depending upon whether the flow is subsonic or supersonic. The truncation error of the difference scheme has the effect of artificial viscosity, so shock waves appear naturally during the course of calculation, although they are usually spread over 3–4 mesh points. The system of difference equations is solved by successive line relaxation, and the computed results agree well with experimental data for a circular arc airfoil.

The method was extended by Krupp & Murman (1972) to lifting airfoils and slender bodies. Steger & Lomax (1972) solved the full potential equations for lifting airfoils by successive line over-relaxation (SLOR). An interactive graphic terminal is used to change the values of circulation and relaxation parameters as the relaxation is proceeding. To account for flows not aligned to the co-ordinate system, Jameson (1974) introduced a rotated differencing scheme in which the direction of upwind differencing is rotated to conform with the local flow direction. The system of difference equations is then iterated by simulating an artificial time-dependent equation. Ballhaus, Jameson & Albert (1978) developed an implicit approximate factorization (AF) algorithm for the solution of steady-state transonic small-disturbance equation, which has a much better rate of convergence than the SLOR algorithm. Following the idea of Jameson's rotating upwind difference scheme, Holst & Ballhaus (1979) solved the full potential equation in conservation form to ensure conservative shock capturing. Artificial viscosity is added implicitly by retarding the density according to local Mach number. Holst (1979) later applied the method using an arbitrary mesh, and obtained good agreement with independently computed results.

The hodograph method has a long history in transonic flow calculations, taking advantage of the property that the governing equations of plane motion become linear when co-ordinates in the physical plane are replaced by the velocity components as independent variables. Using the hodograph transformation, Nieuwland (1967) developed a technique for computing shock-free, symmetrical, supercritical flows about quasi-elliptic airfoil sections. The method was later extended by Boerstoel (1967) to present a catalogue of solutions for certain body shapes. Bauer, Garabedian & Korn (1972) also used the hodograph method to generate a shock-free flow with the corresponding boundary shapes.

The final category of the methods makes use of quasi-analytic techniques. These are the 'method of integral relations' (MIR), Telenin's method and the 'method of lines' (see Holt 1977). Each approach uses smooth interpolating functions to represent the unknown variables in a selected co-ordinate direction. The partial differential equations are thereby reduced to a set of ordinary differential equations along a set of rays in the flow field. The resulting equations are then solved as an initial-value problem.

MIR was first applied by Chushkin (1958) for subsonic critical flow past an ellipse or ellipsoid. Later, Holt & Masson (1971) computed supercritical flow about a cylinder with the full potential equations. Tai (1974) also used MIR to solve the steady Euler equations for a lifting airfoil. Both of the above methods located a shock point on the body, but no details about the shape of the shock in the interior of the flow field are obtained.

Chattot (1978) applied Telenin's method in the hodograph plane for flow past a

double wedge. A shock is fitted in the flow field to eliminate the limit lines. The complete shock location is obtained, but the method is restricted to a double wedge, where the boundaries in the hodograph plane are known in advance. Telenin's method was also used by Gross & Holt (1976) to calculate critical and supercritical shock-free flow past ellipses.

In the present work supercritical flow past an ellipse at zero angle of attack is calculated. The steady two-dimensional full potential equations are solved by Telenin's method and the method of lines. The jump conditions of the equations are used to fit a shock in the flow field to terminate the supersonic region. The formulation of the equations of motion and the details of the transonic flow field are discussed in §2. Applications of Telenin's method and the method of lines to the supercritical flow problem are described in §3. Section 4 contains discussions of the supercritical calculations. The conclusions are presented in §5.

2. Formulation of the problem

We consider the two-dimensional flow of a uniform stream past an ellipse. The free-stream Mach number lies in the high subsonic range so that, while the flow in the region far from the ellipse is wholly subsonic, the flow field in the neighbourhood of the ellipse is of mixed type with subsonic regions near the forward and rear stagnation points and a local supersonic region near the maximum thickness section of the ellipse. The local supersonic region is usually bounded by a shock wave at its downstream end. A typical flow pattern is shown in figure 2(*b*).

Viscosity effects are confined to the boundary layer near the surface of the ellipse. The boundary-layer calculations will be carried out subsequently since these require knowledge of the inviscid flow field as a starting point. The shock terminating the local supersonic region causes the boundary layer to separate so that the inviscid and viscous flows interact significantly. However, the main influence of boundary-layer separation is to introduce an effective thickening of the ellipse downstream of the shock. Interaction effects are therefore determined by integrating the inviscid and boundary-layer equations separately and matching the calculations along the effective viscous–inviscid boundary.

The shock wave introduces entropy changes on its downstream side. Provided that the minor-axis–major-axis ratio (maximum thickness ratio) of the ellipse is sufficiently small and provided that the free-stream Mach number is subsonic, the local Mach number ahead of the shock wave will not exceed the value 1·3. The shock wave strength is then sufficiently small to ensure that entropy changes can be neglected.

To verify this statement we use the following perfect-gas relationship to determine entropy changes across a shock wave:

$$\frac{\Delta S}{R} = \frac{1}{\gamma-1}\ln\left[\frac{2\gamma M^2-\gamma+1}{\gamma+1}\right] - \frac{\gamma}{\gamma-1}\ln\left[\frac{(\gamma+1)M^2}{(\gamma-1)M^2+2}\right]. \tag{2.1}$$

Here, M is the incident Mach number (just upstream of the shock), γ the ratio of specific heats, R the gas constant, and ΔS the change in entropy. If $M = 1{\cdot}3$ and $\gamma = 1{\cdot}4$, then

$$\frac{\Delta S}{R} = 0{\cdot}0208. \tag{2.2}$$

Equation (2.1) can be rewritten as

$$p_2 = p_1 \left(\frac{\rho_2}{\rho_1}\right)^{\gamma} \left[\exp\left(\frac{\Delta S}{R}\right)\right]^{(\gamma-1)}, \tag{2.3}$$

where p is the pressure and ρ the density. Subscripts 1 and 2 denote conditions ahead of and behind the shock, respectively.

From equation (2.2)

$$\left[\exp\left(\frac{\Delta S}{R}\right)\right]^{(\gamma-1)} = 1{\cdot}0084. \tag{2.4}$$

It follows that for shocks with incident Mach numbers $M < 1{\cdot}3$ the error introduced by the isentropic assumption is about 0·8 %. We can therefore assume, in the present analysis, that the flow field is isentropic and irrotational.

2.1. *Equations of motion*

We consider steady, two-dimensional flow of a uniform air stream past an ellipse at high subsonic free-stream Mach numbers. The flow is assumed to be inviscid and irrotational. The governing equations of motion are then:

Coniinuity $$\operatorname{div}(\rho \mathbf{q}) = 0; \tag{2.5}$$

Irrotationality $$\operatorname{curl}(\mathbf{q}) = 0. \tag{2.6}$$

Writing these equations in elliptic co-ordinates:

$$\frac{\partial(\rho u h)}{\partial \xi} + \frac{\partial(\rho v h)}{\partial \eta} = 0, \quad \frac{\partial(v h)}{\partial \xi} - \frac{\partial(u h)}{\partial \eta} = 0. \tag{2.7), (2.8}$$

The elliptic co-ordinates ξ and η are defined by (Milne-Thomson 1972):

$$x = c \cosh \xi \cos \eta, \quad y = c \sinh \xi \sin \eta, \tag{2.9), (2.10}$$

where x and y are Cartesian co-ordinates, c is a constant, u and v are the velocity components in the ξ and η directions, respectively, and h is the metric coefficient given by:

$$h = c(\sinh^2 \xi + \sin^2 \eta)^{\frac{1}{2}}. \tag{2.11}$$

It can be shown that curves of constant ξ represent confocal ellipses and curves of constant η confocal hyperbolae. The foci of the ellipses or hyperbolae are located at $(\pm c, 0)$. Some curves of the elliptic co-ordinate system with $c = 1$ are plotted in figure 1.

The final equation to complete the set is Bernoulli's equation:

$$H + \tfrac{1}{2}q^2 = H_0 = \tfrac{1}{2}q_{\max}^2. \tag{2.12}$$

The quantity H is the enthalpy (per unit mass), q is the flow speed, $q_{\max}$ the maximum steady expansion speed, and the subscript 0 denotes stagnation conditions. Equation (2.12) may be written

$$\frac{H}{H_0} = 1 - \left(\frac{q}{q_{\max}}\right)^2. \tag{2.13}$$

For a perfect gas with constant specific heats

$$H = \frac{\gamma p}{(\gamma - 1)\rho}. \tag{2.14}$$

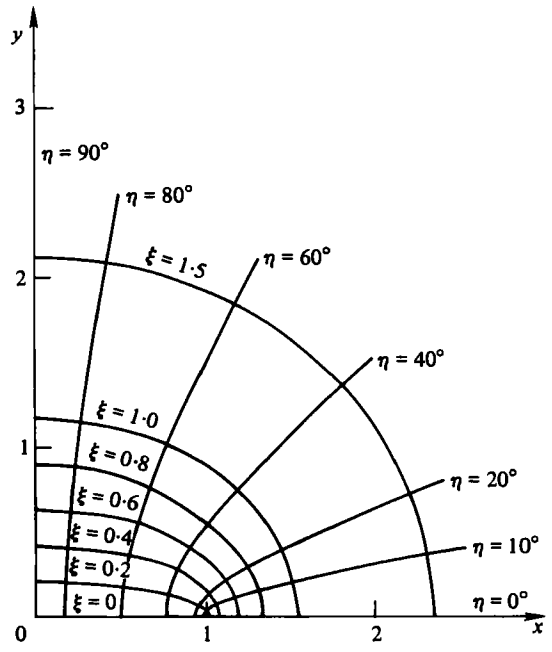

FIGURE 1. Elliptic co-ordinates in the first quadrant with foci located at (± 1, 0).

By further assuming isentropic flow

$$p \propto \rho^{\gamma} \tag{2.15}$$

it follows that

$$\frac{H}{H_0} = \frac{p}{p_0}\frac{\rho_0}{\rho} = \left(\frac{\rho}{\rho_0}\right)^{\gamma-1}. \tag{2.16}$$

Substituting equation (2.16) into (2.13) and solving for ρ/ρ_0, we obtain

$$\frac{\rho}{\rho_0} = \left(1-\left(\frac{q}{q_{\max}}\right)^2\right)^{1/(\gamma-1)}. \tag{2.17}$$

The three equations (2.7), (2.8) and (2.17) are the three relations required to determine the three basic unknowns u, v and ρ.

We now express all variables in dimensionless form by dividing distances by c, velocities by $q_{\max}$, and the density by the stagnation density ρ_0. Retaining the same symbols for the non-dimensional variables, the equations of motion are

$$\frac{\partial(\rho u h)}{\partial \xi}+\frac{\partial(\rho v h)}{\partial \eta} = 0, \quad \frac{\partial(v h)}{\partial \xi}-\frac{\partial(u h)}{\partial \eta} = 0, \tag{2.18), (2.19}$$

$$\rho = (1-q^2)^{1/(\gamma-1)} = (1-u^2-v^2)^{1/(\gamma-1)} \tag{2.20}$$

and

$$h = (\sinh^2\xi+\sin^2\eta)^{\frac{1}{2}}, \tag{2.21}$$

$$x = \cosh\xi\cos\eta, \quad y = \sinh\xi\sin\eta. \tag{2.22), (2.23}$$

2.2. *Description of the flow field*

Before we proceed to solve the equations of motion, it is advantageous to understand the physical flow field and be able to choose an effective method to solve the problem.

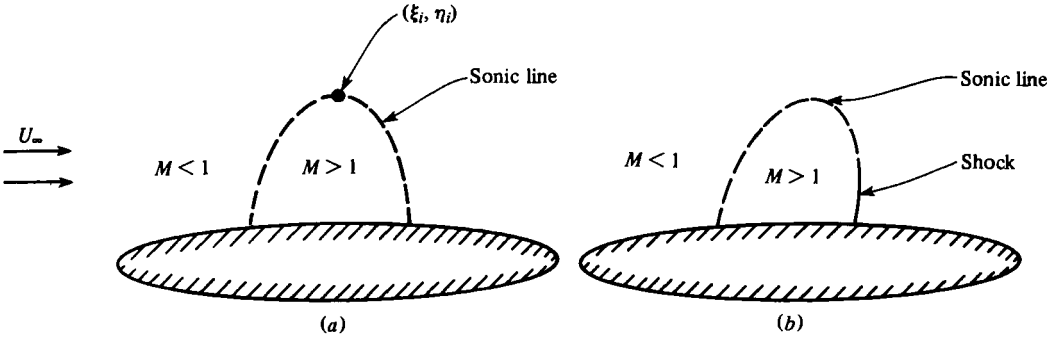

FIGURE 2. (*a*) Unstable supercritical shock-free flow field and (*b*) typical supercritical flow field.

At very low Mach numbers, the compressibility is very small, hence the flow can be assumed to be incompressible. The analytic solution for incompressible flow past an elliptic cylinder (Milne-Thomson 1972) is given by

$$u = \frac{U_\infty}{h} e^{\xi_0} \cos\eta \sinh(\xi - \xi_0), \quad v = -\frac{U_\infty}{h} e^{\xi_0} \sin\eta \cosh(\xi - \xi_0), \quad (2.24), (2.25)$$

where U_∞ is the free-stream velocity and ξ_0 the ellipse representing the body of the cylinder. On the body, the normal component u of the velocity is zero, and the tangential velocity is given by equation (2.25). It can be seen that the flow accelerates from stagnation at the leading edge ($\eta = \pi$) to a maximum speed at the apex of the cylinder ($\eta = \frac{1}{2}\pi$), and then decelerates back to stagnation at the trailing edge ($\eta = 0$). At zero angle of attack, the flow is symmetric about both the y axis and the x axis.

As the free-stream Mach number is increased, compressibility effects become more important, and the compressible equations of motion have to be solved. However, the flow behaviour remains qualitatively the same if the flow is subsonic throughout the field. When the maximum local Mach number reaches the value 1·0, the flow is said to be critical. The free-stream Mach number which produces such a flow is called the critical free-stream Mach number.

For supercritical flow, a small supersonic region is embedded in the subsonic flow field. Although shock-free supercritical flows can be produced, they are generally unstable (see Busemann 1949; Frankl 1950; Guderley 1953; Morawetz 1956, 1957) in the sense that a small perturbation of the body contour in the supersonic region leads to a flow that is discontinuous. This will be assumed the case for our transonic flow calculation. A typical transonic flow field is depicted in figure 2(*b*).

3. Numerical methods

Telenin's method and the 'method of lines' are used as the numerical schemes to solve the equations of motion. The two methods are very similar. In Telenin's method the variations of the variables in one co-ordinate direction are represented by some smooth interpolating functions. In our problem, symmetry conditions suggest the use of Fourier series of the form:

$$u(\xi, \eta) = \sum_{i=1}^{N} a_i(\xi) \cos(i-1)\eta, \quad v(\xi, \eta) = \sum_{i=1}^{N-2} b_i(\xi) \sin i\eta, \quad (3.1), (3.2)$$

where N is the number of rays. Along the jth ray

$$u_j = u(\xi, \eta_j) = \sum_{i=1}^{N} a_i(\xi) \cos(i-1)\eta_j. \tag{3.3}$$

The coefficient a_i can be obtained by inverting the matrix $\{\cos(i-1)\eta_j\}$,

$$a_i = \sum_{j=1}^{N} A_{ij} u_j, \quad i = 1, \ldots, N, \tag{3.4}$$

where $\{A_{ij}\} = \{\cos(j-1)\eta_i\}^{-1}$. Equation (3.1) is differentiated to obtain the η derivatives, giving

$$\left(\frac{\partial u}{\partial \eta}\right)_l = \frac{\partial u(\xi, \eta_l)}{\partial \eta} = \sum_{i=1}^{N} a_i(\xi)(1-i)\sin(i-1)\eta_l. \tag{3.5}$$

Substituting equation (3.4) into (3.5) yields

$$\left(\frac{\partial u}{\partial \eta}\right)_l = \sum_{i=1}^{N} \left(\sum_{j=1}^{N} A_{ij} u_j\right)(1-i)\sin(i-1)\eta_l. \tag{3.6}$$

Interchanging the order of operation,

$$\left(\frac{\partial u}{\partial \eta}\right)_l = \sum_{j=1}^{N} \left(\sum_{i=1}^{N} A_{ij}(1-i)\sin(i-1)\eta_l\right) u_j = \sum_{j=1}^{N} F_{lj} u_j. \tag{3.7}$$

Similarly, for the derivative of v

$$\left(\frac{\partial v}{\partial \eta}\right)_l = \sum_{j=1}^{N-2} G_{lj} v_j, \quad l = 1, 2, \ldots, N, \tag{3.8}$$

where

$$F_{lj} = \sum_{i=1}^{N} A_{ij}(1-i)\sin(i-1)\eta_l, \quad G_{lj} = \sum_{i=1}^{N-2} B_{ij}\, i \cos i\eta_l, \tag{3.9), (3.10}$$

and where

$$\{B_{ij}\} = \{\sin i\eta_{j+1}\}^{-1}. \tag{3.11}$$

In the 'method of lines', the η derivatives are approximated by finite differences. Three-point or five-point difference schemes are used depending on the order of accuracy required. The derivative representation has the same form as given by (3.7) with coefficients F_{ij} derived from Taylor series expansions. Hence in terms of the solution method and accuracy, we may consider the two methods to be equivalent.

It is convenient to have expressions for $\partial v/\partial \xi$ and $\partial u/\partial \xi$. From equation (2.19)

$$v\frac{\partial h}{\partial \xi} + h\frac{\partial v}{\partial \xi} = u\frac{\partial h}{\partial \eta} + h\frac{\partial u}{\partial \eta}. \tag{3.12}$$

Solving for $\partial v/\partial \xi$:

$$\frac{\partial v}{\partial \xi} = \frac{1}{h}\left(u\frac{\partial h}{\partial \eta} + h\frac{\partial u}{\partial \eta} - v\frac{\partial h}{\partial \xi}\right). \tag{3.13}$$

The definition of h implies that

$$\frac{\partial h}{\partial \xi} = \frac{\sinh 2\xi}{2h}, \quad \frac{\partial h}{\partial \eta} = \frac{\sin 2\eta}{2h}. \tag{3.14), (3.15}$$

The above expressions are substituted into (3.13) to give

$$\frac{\partial v}{\partial \xi} = \frac{\partial u}{\partial \eta} + \frac{u \sin 2\eta}{2h^2} - \frac{v \sinh 2\xi}{2h^2}. \tag{3.16}$$

From equations (2.18) and (2.20), we obtain

$$\frac{u}{h}\frac{\partial h}{\partial \xi}+\frac{\partial u}{\partial \xi}+\frac{u}{\rho}\frac{\partial \rho}{\partial \xi}=-\frac{1}{\rho h}\frac{\partial(\rho v h)}{\partial \eta}, \tag{3.17}$$

and

$$\frac{1}{\rho}\frac{\partial \rho}{\partial \xi}=-\frac{2\left[u\dfrac{\partial u}{\partial \xi}+v\dfrac{\partial v}{\partial \xi}\right]}{(\gamma-1)(1-u^2-v^2)}. \tag{3.18}$$

Substituting (3.18) into (3.17) and solving for $\partial u/\partial \xi$, gives

$$\frac{\partial u}{\partial \xi}=\frac{P_1}{Q_1}, \tag{3.19}$$

where

$$P_1=2uv\left(\frac{\partial v}{\partial \xi}+\frac{\partial u}{\partial \eta}\right)+2v^2\frac{\partial v}{\partial \eta}-(\gamma-1)(1-u^2-v^2)\left(\frac{\partial v}{\partial \eta}+\frac{v\sin 2\eta}{2h^2}+\frac{u\sinh 2\xi}{2h^2}\right), \tag{3.20}$$

$$Q_1=(\gamma-1)(1-v^2)-(\gamma+1)u^2. \tag{3.21}$$

Substitution of expressions (3.7) and (3.8) into (3.16) and (3.19) results in a system of $(2N-2)$ ordinary differential equations that can be integrated simultaneously in the ξ direction, along N rays of constant η.

3.1. *Boundary conditions*

Boundary conditions have to be prescribed in order to specify the problem uniquely. On the body, we require that normal velocity be zero, that is

$$u=0 \quad \text{for} \quad \xi=\xi_0, \tag{3.22}$$

where ξ_0 is the elliptic co-ordinate of the body. For flow past an elliptic cylinder at zero angle of attack, the flow field is symmetric about the x axis, so

$$v=0, \quad \frac{\partial u}{\partial \eta}=0 \quad \text{for} \quad \eta=0,\pi. \tag{3.23}$$

Finally, the flow approaches that of a uniform free stream at infinity:

$$u\to U_\infty\cos\eta, \quad v\to -U_\infty\sin\eta \quad \text{as} \quad \xi\to\infty. \tag{3.24}$$

However, in practice, it is more convenient to specify the far-field boundary conditions at a finite distance from the body. Following Murman & Cole (1971), an analytical solution for the far field is derived using transonic small-disturbance theory. The basic transonic equation is

$$[K\phi_x-\tfrac{1}{2}(\gamma+1)\phi_x^2]_x+\phi_{\tilde{y}\tilde{y}}=0 \tag{3.25}$$

with the variables and parameters defined by

$$\tilde{y}=\delta^{\frac{1}{2}}y, \quad K=(1-M_\infty^2)/\delta^{\frac{1}{3}}, \tag{3.26), (3.27}$$

$$\frac{q_x}{U_\infty}=1+\delta^{\frac{2}{3}}q_x'+\ldots, \quad \frac{q_y}{U_\infty}=\delta q_y'+\ldots, \tag{3.28), (3.29}$$

and the perturbation velocities are

$$q'_x = \phi_x, \quad q'_y = \phi_{\tilde{y}}. \tag{3.30}$$

Here δ is the thickness ratio of the airfoil (or ellipse), M_∞ the free-stream Mach number, q_x and q_y are the velocity components in the x and y directions, respectively.

We rewrite equations (3.25) in the form

$$L\phi \equiv K\phi_{xx} + \phi_{\tilde{y}\tilde{y}} = \tfrac{1}{2}(\gamma+1)(u^2)_x. \tag{3.31}$$

Applying Green's formula for L in the upper half-plane and allowing for a shock jump in the flow field, we obtain the basic integral equation

$$\begin{aligned}\phi(x,\tilde{y}) = {} & \frac{1}{\pi K^{\frac{1}{2}}}\int_{-1}^{+1} \frac{x-x'}{(x-x')^2+K\tilde{y}^2} F(x')\,dx' \\ & + \frac{\gamma+1}{2}\frac{1}{2\pi K^{\frac{1}{2}}}\iint_{-\infty}^{\infty} \frac{(x-x')\{q'_x(x',y')\}^2}{(x-x')+K(\tilde{y}-y)^2}\,dx'\,dy'.\end{aligned} \tag{3.32}$$

The far field is thus that of the usual doublet for a closed body

$$\phi(x,\tilde{y}) \simeq \frac{D}{2\pi K^{\frac{1}{2}}}\frac{x}{(x^2+K\tilde{y}^2)} + \ldots, \tag{3.33}$$

where the doublet strength is

$$D = 2\int_{-1}^{1} F(x)\,dx + \tfrac{1}{2}(\gamma+1)\iint_{-\infty}^{\infty} \{q'_x(x,y)\}^2\,dx\,dy. \tag{3.34}$$

The doublet strength consists of the usual term proportional to the airfoil volume and a nonlinear contribution, unknown in advance. In the numerical procedure D has to be calculated as one of the unknowns of the problem. Differentiating equation (3.33) gives

$$q'_x = \frac{D}{2\pi K^{\frac{1}{2}}}\frac{(-x^2+K\tilde{y}^2)}{(x^2+K\tilde{y}^2)^2}, \quad q'_y = -\frac{DK^{\frac{1}{2}}}{\pi}\frac{xy}{(x^2+K\tilde{y}^2)^2}. \tag{3.35), (3.36}$$

The flow velocities expressed in the ξ and η directions are given by

$$u = \frac{1}{h}(q_x \sinh\xi\cos\eta + q_y \cosh\xi\sin\eta), \tag{3.37}$$

$$v = \frac{1}{h}(-q_x \cosh\xi\sin\eta + q_y \sinh\xi\cos\eta). \tag{3.38}$$

Substitution of equations (3.28) and (3.29) into (3.37) and (3.38) gives the necessary boundary conditions in the far field.

3.2. *Jump conditions*

For transonic flow at sufficiently high, subsonic, free-stream Mach number, the flow becomes supercritical. A region of local supersonic flow is developed over the maximum thickness region of the body and this is terminated on the downstream side by a shock wave. In the inviscid flow approximation, the shock wave is modelled by a jump discontinuity in the solution. To ensure uniqueness, we require that entropy increases across the shock wave. For the full potential approximation, the entropy change is assumed to be negligible. Uniqueness is attained by allowing only the existence of

compression shocks, but not expansion shocks. The jump conditions for the full potential equations are different from the usual Rankine–Hugoniot relations, and can be derived by writing the equations of motion in conservation form. Applying the two-dimensional form of the divergence theorem to equations (2.18) and (2.19), we obtain

$$\langle \rho uh \rangle (d\eta)_s - \langle \rho vh \rangle (d\xi)_s = 0, \tag{3.39}$$

and

$$\langle vh \rangle (d\eta)_s + \langle uh \rangle (d\xi)_s = 0, \tag{3.40}$$

where $\langle\ \rangle$ denote a jump in the quantity across the shock and subscript s denotes an element in the shock surface. Equations (3.39) and (3.40) can be rewritten as

$$\langle \rho uh \rangle \eta_s' - \langle \rho vh \rangle = 0, \quad \langle vh \rangle \eta_s' + \langle uh \rangle = 0, \tag{3.41), (3.42}$$

where

$$\eta_s' = \left(\frac{d\eta}{d\xi}\right)_s \tag{3.43}$$

is the shock wave angle. In equations (3.41) and (3.42) h is the metric coefficient which depends only on the geometry of the co-ordinate system and is continuous throughout the field, and hence can be eliminated from (3.41) and (3.42). The final form of the jump conditions is then

$$\langle \rho u \rangle \eta_s' - \langle \rho v \rangle = 0, \quad \langle v \rangle \eta_s' + \langle u \rangle = 0. \tag{3.44), (3.45}$$

Equations (3.44) and (3.45) represent, respectively, the conservation of mass flux and continuity of tangential velocity across the shock wave. The density ρ in (3.44) is given by Bernoulli's equation (2.20). Thus the jump conditions for the full potential equations are completely specified.

It is interesting to compare the shock-fitting and shock-capturing methods. In the finite-difference treatment of supercritical flow, artificial viscosity is added to the differential equations as a result of the truncation errors generated by the difference equations. No explicit jump conditions are needed, provided that the equations are written in divergence form to conserve mass flux. Shock waves evolve naturally during the course of the calculation, although they usually spread over several mesh points. In principle, the shock wave can be made arbitrarily sharp by refining the mesh points near to it; however, this will slow down the rate of convergence considerably. By employing a shock-fitting technique, the jump conditions are satisfied exactly. The shock wave is perfectly sharp, hence no refinement is necessary. The drawback of this method is that the iteration may not converge if the initial guess of the shock location is too inaccurate.

3.3. *Singular points*

At the beginning of §3, we assumed a Fourier series representation in the η direction for the unknown flow quantities, and, as a result, derived a set of first-order ordinary differential equations (equations (3.16) and (3.19)) in the ξ direction. However, it is also possible to assume an analytic representation in the ξ direction and obtain a set of ordinary differential equations in the η direction. The advantages and disadvantages of each formulation will become apparent at a later stage.

For the latter formulation, we must derive expressions for $\partial u/\partial \eta$ and $\partial v/\partial \eta$. Rearranging equations (2.18) and (2.19), and solving for $\partial v/\partial \eta$ and $\partial u/\partial \eta$, we obtain

$$\frac{\partial u}{\partial \eta} = \frac{\partial v}{\partial \xi} + \frac{v \sinh 2\xi}{2h^2} - \frac{u \sin 2\eta}{2h^2}, \quad \frac{\partial v}{\partial \eta} = \frac{P_2}{Q_2}, \tag{3.46), (3.47}$$

where

$$P_2 = 2uv\left(\frac{\partial u}{\partial \eta}+\frac{\partial v}{\partial \xi}\right)+2u^2\frac{\partial u}{\partial \xi}-(\gamma-1)(1-u^2-v^2)\left(\frac{\partial u}{\partial \xi}+\frac{u\sinh 2\xi}{2h^2}+\frac{v\sin 2\eta}{2h^2}\right), \quad (3.48)$$

$$Q_2 = (\gamma-1)(1-u^2)-(\gamma+1)v^2. \quad (3.49)$$

When equations (3.16) and (3.19) are examined in detail, it is observed that they have a saddle-point singularity when the denominator Q_1 becomes zero, that is,

$$(\gamma-1)(1-v^2)-(\gamma+1)u^2 = 0. \quad (3.50)$$

After rearranging, we obtain

$$\frac{u^2}{(\gamma-1)/(\gamma+1)}+v^2 = 1, \quad (3.51)$$

which represents an ellipse in the u, v plane. From Bernoulli's equation,

$$q^2 = \frac{(\gamma-1)M^2}{2+(\gamma-1)M^2}, \quad (3.52)$$

so the non-dimensional critical velocity q^* is

$$q^{*2} = (\gamma-1)/(\gamma+1). \quad (3.53)$$

On substituting equation (3.53) into (3.51), the ellipse of singularities may be written as

$$\frac{u^2}{q^{*2}}+\frac{v^2}{1} = 1. \quad (3.54)$$

The singular ellipse and the sonic circle are both plotted in figure 3(*a*). We can see that all points on the ellipse lie outside the sonic circle, except for $v = 0$, $u = \pm q^*$. For critical flow, only one point is on the sonic circle, namely $u = 0$, $v = \pm q^*$, therefore there are no singularities for a critical-flow calculation when integrating away from the body. It is apparent that no singularities will be encountered even for supercritical flow calculations.

On the other hand, using the second formulation and integrating in the η direction, the denominator of (3.47) becomes zero when

$$(\gamma-1)(1-u^2)-(\gamma+1)v^2 = 0. \quad (3.55)$$

Hence the singular ellipse in the u, v plane is given by

$$u^2+\frac{v^2}{q^{*2}} = 1, \quad (3.56)$$

which is shown in figure 3(*b*). But any critical or supercritical flow has a point on the body with $u = 0$ and $v = -q^*$, which is a point on the ellipse given by (3.56). Therefore it is obvious that integration in the η direction always leads to at least one singularity at sonic points on or near the body.

3.4. *Implementation of the numerical scheme*

As discussed in the preceding section, saddle-point singularities will arise if we assume interpolating functions in the ξ direction. Hence it will be appropriate to use the first formulation given at the beginning of §3. Expressions (3.7) and (3.8) are substituted into (3.16) and (3.19) to form a set of $(2N-2)$ simultaneous ordinary differential

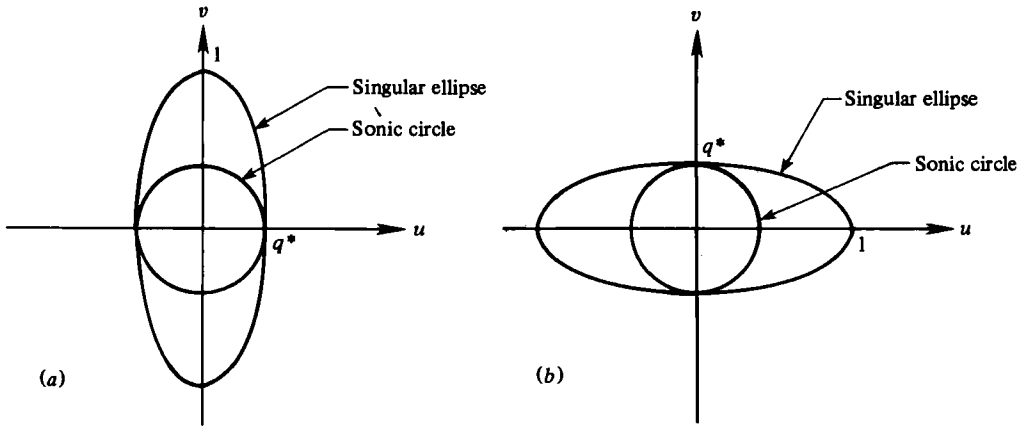

FIGURE 3. Singular ellipse for (*a*) first formulation and (*b*) second formulation.

equations. At $\xi = \xi_0$, the flow tangency condition on the body is given by (3.22). An initial estimate of values of the tangential velocities v_0 on the surface is made, and, using these as initial data, the equations are integrated away from the ellipse $\xi = \xi_0$. A variable-step, fifth-order Runge–Kutta method is used to integrate the differential equations. The integration is terminated at a distance sufficiently far away from the body, say $\xi = \xi_\infty$, which will be defined later. The velocities v calculated at ξ_∞ are then compared with the far-field velocities given by (3.38). If the two sets of values differ, tangential velocities on the surface are then adjusted and the integration is repeated. The procedure is repeated until the far-field solution converges. This can be done very efficiently by the use of Powell's method (Powell 1964), which minimizes the sum of squares of the differences between the far-field velocities by adjusting the surface velocities. The iteration is terminated when the sum satisfies the specified tolerance.

Gilinskii, Telenin & Tinyakov (1964) pointed out that solving a Dirichlet problem as a Cauchy problem is inherently unstable with respect to the prescribed data. This phenomenon is known as Hadamard instability. Jones, South & Klunker (1972) also encountered Hadamard instability in applying the 'method of lines' and found growth in error proportional to $\exp(N\xi)$, where N is the number of rays and ξ the direction of integration. As a consequence, the number of rays and the far-field distance have to be restricted. However, if we wish to obtain a solution with reasonable accuracy, we must employ a sufficient number of rays to represent the variables. The occurrence of a shock wave on the body makes it even more desirable to have a detailed representation near the body.

To overcome the above difficulties, we propose to solve the problem in two stages. In the first stage, a very coarse representation of the variables is used, which enables us to integrate the equations away from the body to the far field without instability problems. A supercritical shock-free flow is obtained from this calculation. However, as discussed in §2.2, shockless flows are known to be unstable and not likely to occur in practical situations. Hence, in our supercritical flow calculation, we always assume that the flow is discontinuous. In order to model the shock wave, we have to treat the region near the body in a different manner. The procedure for the different stages is described in the following sections.

(*a*) *Coarse solution*

In this stage, we assume Fourier series representation of the form (3.1) and (3.2) for u and v. For flow over an ellipse, we further notice that the flow is symmetric about the y axis when the solution is smooth. Thus we can economize on the number of rays by assuming series of the form:

$$u(\xi,\eta) = \sum_{i=1}^{N-1} a_i(\xi)\cos(2i-1)\eta, \quad v(\xi,\eta) = \sum_{i=1}^{N-1} b_i(\xi)\sin(2i-1)\eta. \quad (3.57), (3.58)$$

So for the coarse solution, we only need to compute the flow in the second quadrant. Equations (3.16) and (3.19) are integrated simultaneously from ξ_0 to ξ_∞. Boundary conditions are satisfied by using the procedure described in §3.4. At supercritical Mach number, a continuous flow with a small embedded supersonic zone is obtained, and is depicted in figure 2(*a*).

(*b*) *Refined solution near the body*

Although the coarse solution does not have enough accuracy to resolve the shock wave which occurs near the body, it provides a fairly good representation of the flow field away from the body where the flow is smooth. The strategy here is to use a larger number of rays to represent the flow field close to the body; the coarse solution at an intermediate value of ξ, say ξ_i, is used as the outer boundary condition for the refined solution near the body. In this way, the distance in the ξ direction is kept small and a larger number of rays can be used without causing instabilities.

It is advantageous to integrate the equations in the η direction if we wish to fit a shock in the flow field. Following the idea of Fletcher (1975), we divide the region near the body into two parts. The forward part is enclosed by $\xi = \xi_0$, $\xi = \xi_i$, $\eta = \pi$, and $\eta = \eta_i$, and the rear portion by $\xi = \xi_0$, $\xi = \xi_i$, $\eta = \eta_i$ and $\eta = 0$, which we shall call region 1 and region 2, respectively. The configurations are shown schematically in figures 4 and 5. ξ_i is chosen such that the point (ξ_i, η_i) is at the top of the sonic line (see figure 2*a*). In our case, $\eta_i = \frac{1}{2}\pi$.

In region 1, finite-difference formulae of the form (3.7) and (3.8) are used to calculate the derivatives in the η direction. The ordinary differential equations (3.16) and (3.19) are integrated as in the coarse calculation. No boundary condition is required on $\eta = \frac{1}{2}\pi$; since there is no influence from downstream in a supersonic region, smooth transition through the sonic line will be sufficient for uniqueness. Tangential velocities on the body are adjusted so that velocities v at ξ_i match those of the coarse calculation. Five rays have been used in this region without encountering stability problems.

In region 2, derivatives in the ξ direction are calculated by finite-difference formulae of the following form:

$$\left(\frac{\partial u}{\partial \xi}\right)_l = \sum_{i=1}^{M} E_{li} u_i, \quad \left(\frac{\partial v}{\partial \xi}\right)_l = \sum_{i=1}^{M} H_{li} v_i, \quad (3.59), (3.60)$$

where M is the number of rays, E_{li} and H_{li} are matrices obtained by Taylor series expansion. Expressions (3.59) and (3.60) are substituted into (3.46) and (3.47) to form a set of ordinary differential equations. At $\eta = \frac{1}{2}\pi$ the converged solution from region 1 is used as the initial condition to integrate the equations from $\eta = \frac{1}{2}\pi$ to $\eta = 0$. At $\eta = 0$, the symmetry condition $v = 0$ is imposed. However, in the supersonic region the flow has no forewarning of the downstream conditions and the flow will not be

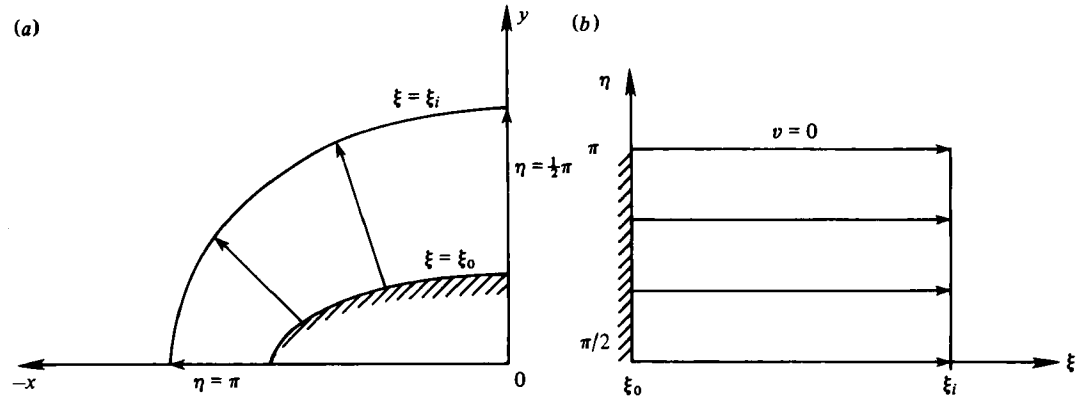

FIGURE 4. Integration in region 1 (*a*) in the physical plane and (*b*) in the ξ, η plane.

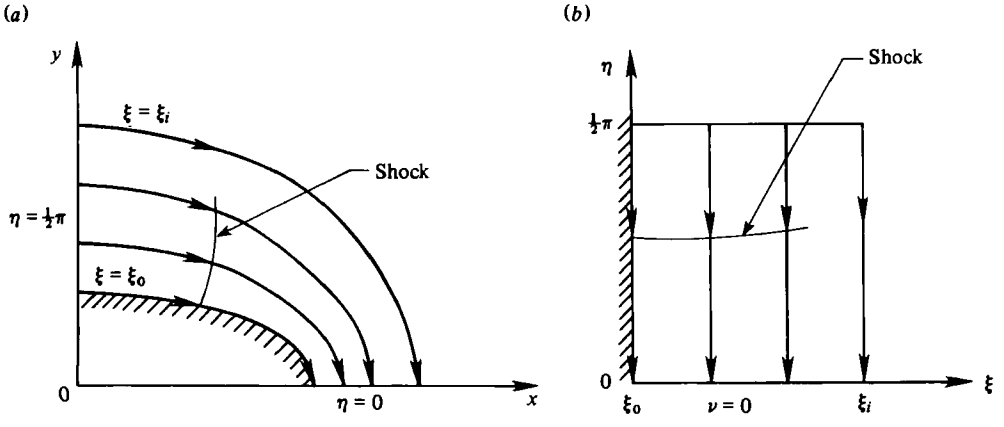

FIGURE 5. Integration in region 2 (*a*) in the physical plane and (*b*) in the ξ, η plane.

able to adjust to satisfy symmetry conditions at $\eta = 0$. Physically, the supersonic region is terminated by a shock wave; the subsonic region behind the shock wave is subsequently compressed to satisfy the boundary condition downstream. To account for the embedded shock wave, the equations are integrated to an intermediate value of η, say $\eta_s(\xi)$, across which jump conditions (3.44) and (3.45) are applied. The integration is then resumed and carried out until $\eta = 0$ is reached. Powell's method is used to adjust the shock location η_s until v becomes zero on $\eta = 0$. The location of the shock is specified by its location on the surface and the shock slope on other rays. It is known, *a priori*, that the local shock shape must be normal to the surface in order to preserve the boundary condition of zero normal flow at the surface.

By splitting the solution domain near the body into two parts, we have been able to integrate the equations of motion in different directions. In the rear part we chose to integrate the equations in the η direction so that a shock can be fitted in the flow field. Since the flow is supersonic ahead of the shock and subsonic behind (at least when boundary-layer interaction effects are not considered), no saddle-point singularity is encountered; thus the integration can be carried out without difficulty. As a word of caution, we note that the shock wave does not extend all the way from the surface to $\xi = \xi_i$ (see figure 2*b*). If we use a large number of rays, the rays of constant ξ with

values close to ξ_i will pass through the sonic line and will cause difficulty if we try to integrate through this line. Therefore care must be taken to ensure that no rays pass through the sonic line.

After a converged solution for region 2 is obtained, the doublet strength D will be re-calculated, and the whole procedure repeated. The solution is considered to have converged globally when the values of D at successive iterations agree to within the prescribed tolerance.

(c) *Powell's method*

To complete the description of our numerical scheme, we shall describe Powell's method briefly; a more detailed analysis can be found elsewhere (see Powell 1964). The method minimizes

$$\sum_{i=1}^{N} \epsilon_i^2 \tag{3.61}$$

with respect to $F_1, F_2, \ldots, F_M$ ($M \leqslant N$), where the N functions ϵ_i are nonlinear functions of the M unknowns F_j. The method is essentially that of least-square minimization in which $\Sigma\epsilon_i^2$ is minimized by making changes to F_j according to the direction $\boldsymbol{\delta F}$ given by

$$\sum_{j=1}^{M} \left\{ \sum_{k=1}^{N} \frac{\partial \epsilon_k}{\partial F_i} \frac{\partial \epsilon_k}{\partial F_j} \right\} \delta F_j = - \sum_{k=1}^{N} \epsilon_k \frac{\partial \epsilon_k}{\partial F_i}, \quad i = 1, 2, \ldots, M. \tag{3.62}$$

New values of $\mathbf{F}$ are given by

$$\mathbf{F} = \mathbf{F}_{\text{old}} + \lambda \boldsymbol{\delta F}, \tag{3.63}$$

in which λ is chosen (by search) such that $\Sigma\epsilon_i^2$ is minimized along the direction $\boldsymbol{\delta F}$. During the search along $\boldsymbol{\delta F}$ to locate the minimum, functions ϵ_i have to be evaluated at different values of λ; thus one can calculate the rate of change of ϵ_i along the direction $\boldsymbol{\delta F}$ at the new minimum point by finite differences. Powell shows how these partial derivatives can be used in conjunction with previous values of $\partial \epsilon_k / \partial P_i$ to determine values for the next step given by (3.62).

In principle the method guarantees convergence since a step is taken only when $\Sigma\epsilon_i^2$ decreases. It also has quadratic convergence provided one is sufficiently near the solution and $\epsilon_i = 0$ at the minimum.

4. Results and discussion

The algorithm introduced in the previous section is evaluated in this section by presenting a range of numerically computed solutions. Ellipses with thickness ratio $\delta = 0{\cdot}4$ and $\delta = 0{\cdot}2$ are chosen for the test cases. Free-stream Mach numbers are assumed to be high enough so that a shock wave will always occur. Gross & Holt (1976) reported critical flow for $\delta = 0{\cdot}4$ at $M_\infty = 0{\cdot}587$. Symmetric, supercritical, shock-free flows were obtained up to $M_\infty = 0{\cdot}644$. A range of free-stream conditions has been chosen for our computations. For thickness ratio $\delta = 0{\cdot}4$, free-stream Mach numbers were chosen to be 0·65, 0·66, 0·67 and 0·68. For $\delta = 0{\cdot}2$, $M_\infty = 0{\cdot}77$. ξ_∞ is assumed to be 2·5, which was found to be sufficiently large by Gross & Holt (1976). Three rays are used for the coarse calculation. When four rays are used, the solution tends to oscillate in the ξ direction at large ξ, which is due to the instability discussed in § 3.4. For region 1 of the refined calculation, five rays are used without encountering instability

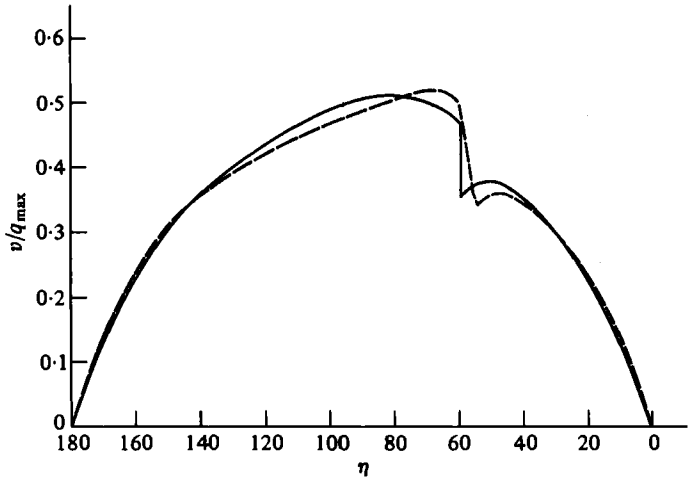

FIGURE 6. Surface velocity distribution, $\delta = 0{\cdot}4$, $M_\infty = 0{\cdot}65$. ———, present method; — — —, Holst method.

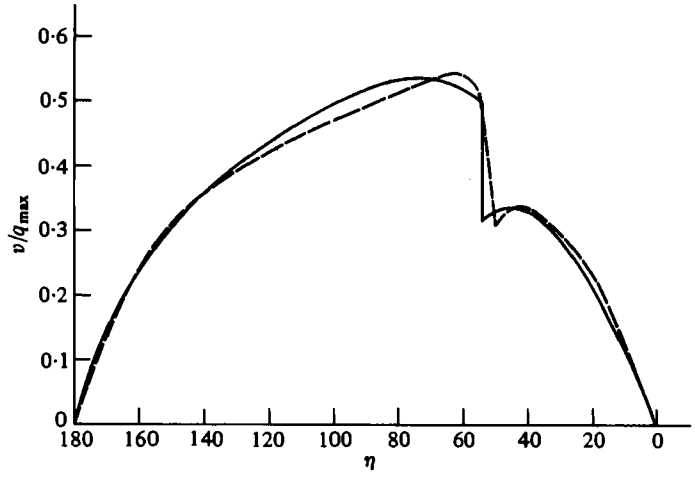

FIGURE 7. Surface velocity distribution, $\delta = 0{\cdot}4$, $M_\infty = 0{\cdot}66$. ———, present method; — — —, Holst method.

problems. However, for region 2 of the refined calculation, only three rays can be used. Besides the instability problem, there are possible singular points in the ordinary differential equations depending on whether or not the rays pass through the sonic points. This is because the shock does not extend all the way out to $\xi = \xi_t$; typically, the top of the shock is located at approximately two-thirds of the distance between ξ_0 and ξ_t. It follows that the use of more than three rays will cause at least one ray to pass through the sonic point, which is hazardous when integrating in the η direction.

The present results are compared with calculations using the shock-capturing method of Holst (1979) and are shown in figures 6–10. For $\delta = 0{\cdot}4$, at $M_\infty = 0{\cdot}65$, 0·66 and 0·67, the two methods agree very well, with the shock locations on the body almost identical. The surface velocity profiles obtained by both methods show similar characteristics. The flow undergoes a small compression before the shock wave is encountered. Behind the shock, a small post-shock expansion wave is observed, after

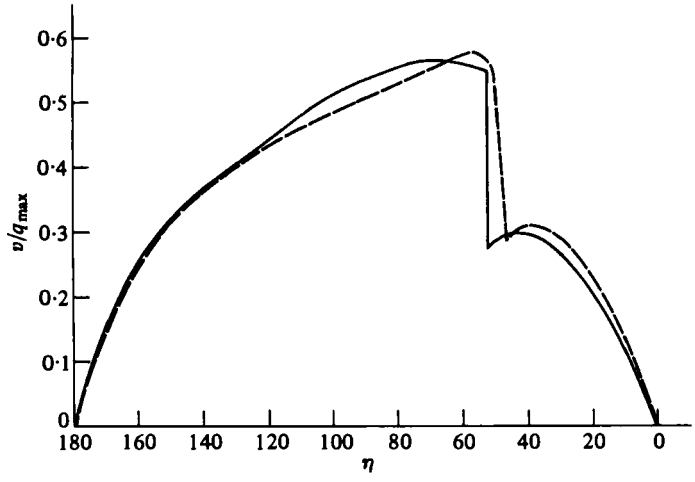

FIGURE 8. Surface velocity distribution, $\delta = 0{\cdot}4$, $M_\infty = 0{\cdot}67$. ———, present method; — — —, Holst method.

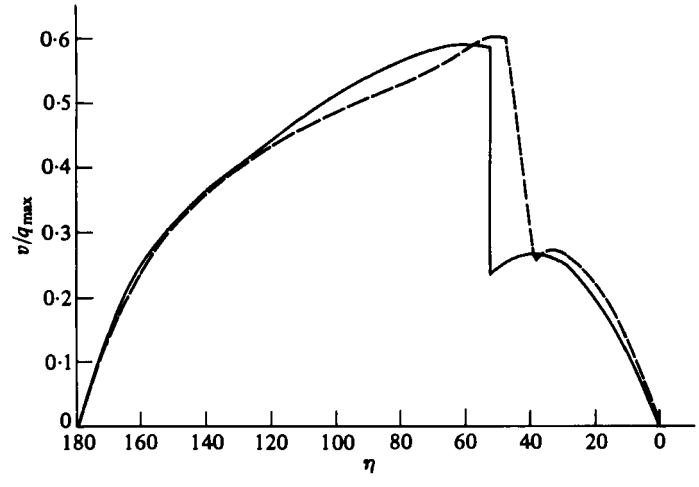

FIGURE 9. Surface velocity distribution, $\delta = 0{\cdot}4$, $M_\infty = 0{\cdot}68$. ———, present method; — — —, Holst method.

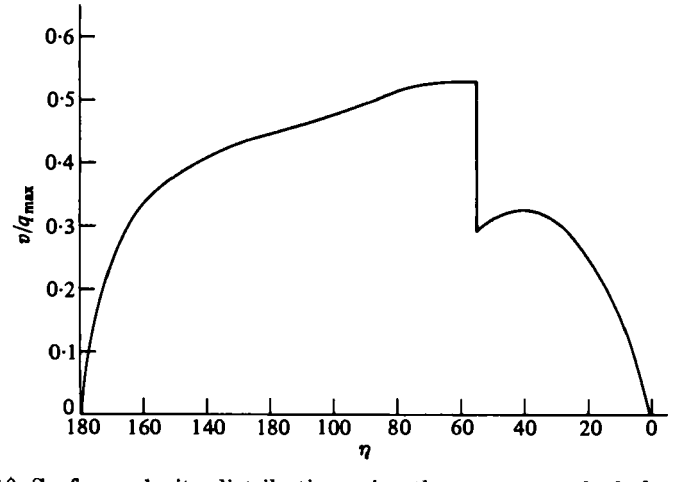

FIGURE 10. Surface velocity distribution using the present method, $\delta = 0{\cdot}2$, $M_\infty = 0{\cdot}77$.

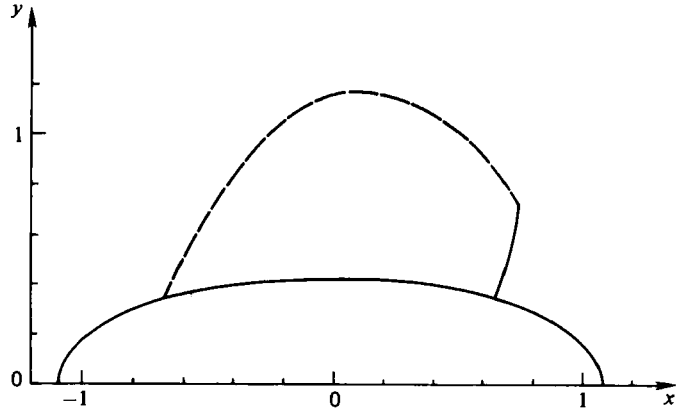

FIGURE 11. Boundary of local supersonic region, $\delta = 0{\cdot}4$, $M_\infty = 0{\cdot}66$.
———, shock; — — —, sonic line.

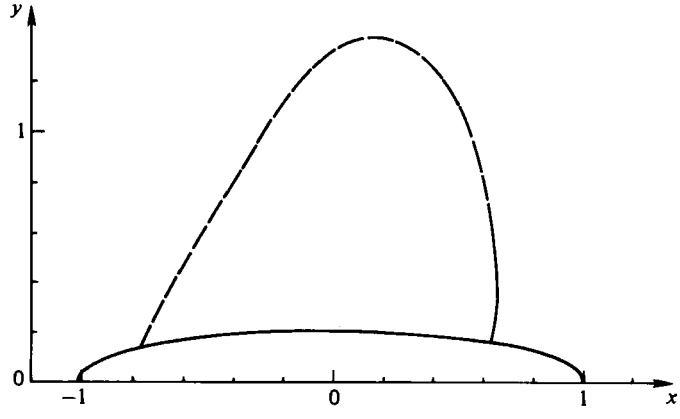

FIGURE 12. Boundary of local supersonic region, $\delta = 0{\cdot}2$, $M_\infty = 0{\cdot}77$.
———, shock; — — —, sonic line.

which the flow is recompressed back to stagnation condition at the trailing edge. The two methods show the largest discrepancies near the shock wave; in all the three cases tested, Holst's method consistently obtains a higher maximum velocity on the body and shows a steeper pre-shock compression. At $M_\infty = 0{\cdot}64$, a solution with an embedded shock wave could not be obtained by the present method. As can be seen in the solution at $M_\infty = 0{\cdot}65$, the shock jump is very weak, and it is quite probable that symmetric shock-free flows exist for free-stream Mach numbers lower than 0·65. However, using Holst's method, a solution with shock jump is obtained for $M_\infty = 0{\cdot}64$. At $M_\infty = 0{\cdot}68$, the solution shows a local Mach number of 1·61 ahead of the shock, the isentropic assumption at this Mach number will introduce an error of about 4·7% according to (2.3) and (2.5). Hence any solutions obtained at or above this free-stream Mach number will be erroneous.

Owing to the unstable nature of the present method, the round-off error grows as $\exp(N\xi)$, where N is the number of rays in the ξ direction. It is difficult to assess the accuracy of the method. Nevertheless, good agreement is obtained between the present method and the shock-capturing method. The present method takes about 3 seconds

to execute on a CDC 7600, whereas Holst's method takes about 6 seconds for a mesh size of 90×40.

Unfortunately, the present method does not guarantee convergence unless the initial guess is reasonably close to the converged solution. One remedy is to increase the free-stream Mach number by a small fraction at a time, say by 0·005, and then use the solution obtained for a previous Mach number as an initial guess. Otherwise, good judgment and trial and error are needed in providing a good initial guess.

5. Conclusions

A composite numerical scheme has been developed which is based in part on Telenin's method and in part on the 'method of lines'. The numerical method has been designed to solve for supercritical flow over an ellipse, when the free-stream Mach number is high enough to generate an embedded shock wave in the flow field. A fitting technique is used to determine this shock so that the Rankine–Hugoniot jump conditions are satisfied exactly across the shock wave.

Good agreement is obtained between the present method and the shock-capturing technique. Further improvement in the present method can be achieved by the introduction of non-symmetrical flow effects into the solution over the forward part of the ellipse. To this end, it is desirable to represent the far-flow-field solution in terms of distributed singularities along the major axis of the ellipse rather than in terms of singularities all located at the ellipse centre.

The work presented in this paper was supported by the U.S. Air Force Office of Scientific Research under Grant No. AFOSR-80-0230.

REFERENCES

BALLHAUS, W. F., JAMESON, A. & ALBERT, J. 1978 Implicit approximate factorization schemes for the efficient solution of steady transonic flow problems. *A.I.A.A. J.* **16**, 573–579.

BAUER, F., GARABEDIAN, P. & KORN, D. 1972 *A Theory of Supercritical Wing Sections, with Computer Program and Examples.* Lecture Notes in Economics and Mathematical Systems, vol. 66. Springer.

BOERSTOEL, J. W. 1967 A survey of symmetrical transonic potential flows around quasi-elliptical aerofoil sections. *Nat. Rep. Aerospace Lab., Amsterdam.* NRL TR T-136.

BUSEMANN, A. 1949 The drag problem at high subsonic speeds. *J. Aero. Sci.* **16**, 337–344.

CHATTOT, J. J. 1978 Symmetrical flow past a double wedge at high subsonic Mach numbers. *J. Fluid Mech.* **86**, 161–177.

CHUSHKIN, P. I. 1958 Subsonic flow of a gas past ellipses and ellipsoids. *Vychislitel'naia Matematika* **2**, 20–24.

FLETCHER, C. A. J. 1975 GTT method applied to cones at large angles of attack. *Proc. 4th Int. Conf. on Numerical Methods in Fluid Dynamics* (ed. R. D. Richtmyer). Lecture Notes in Physics, Vol. 35, pp. 161–166. Springer.

FRANKL, F. I. 1950 On the formation of shocks in subsonic flows with local supersonic velocities. *N.A.C.A. Tech. Memo.* 1251 (translation).

GILINSKII, S. M., TELENIN, G. F. & TINYAKOV, G. P. 1964 A method of computing supersonic flow around blunt bodies, accompanied by a detached shock wave. *Izv. Akad. Nauk, S.S.S.R. Mekh. Mash.* **4**, 9–28. (Also *N.A.S.A. Tech. Transl.* F297, 1965.)

GROSS, M. B. & HOLT, M. 1976 Steady supercritical flow past ellipses. *IUTAM Symp. Transsonicum II, Göttingen, Germany*, 1975 (ed. K. Oswatitsch & D. Rues), pp. 369–375. Springer.

GUDERLEY, G. 1953 Shocks in subsonic–supersonic flow patterns. *Adv. Appl. Mech.* **3**, 145–184.

HOLST, T. L. 1979 Implicit algorithm for the conservative transonic full potential equation using an arbitrary mesh. *A.I.A.A. J.* **17**, 1038–1045.

HOLST, T. L. & BALLHAUS, W. F. 1979 Fast, conservative schemes for the full potential equation applied to transonic flows. *A.I.A.A. J.* **17**, 145–152.

HOLT, M. 1977 *Numerical Methods in Fluid Dynamics.* Series in Computational Physics. Springer.

HOLT, M. & MASSON, B. S. 1971 The calculation of high subsonic flow past bodies by the method of integral relations. *Proc. 2nd Int. Conf. on Numerical Methods in Fluid Mechanics* (ed. M. Holt). Lecture Notes in Physics, vol. 8, pp. 243–251. Springer.

JAMESON, A. 1974 Iterative solution of transonic flows over airfoils and wings, including flows at Mach 1. *Comm. Pure Appl. Math.* **27**, 283–309.

JONES, D. C., SOUTH, J. C. & KLUNKER, E. B. 1972 On the numerical solution of elliptic partial differential equations by the method of lines. *J. Comp. Phys.* **9**, 496–527.

KRUPP, J. A. & MURMAN, E. M. 1972 Computation of transonic flows past lifting airfoils and slender bodies. *A.I.A.A. J.* **10**, 880–881.

MAGNUS, R. & YOSHIHARA, H. 1970 Inviscid transonic flow over airfoils. *A.I.A.A. J.* **8**, 2157–2162.

MILNE-THOMSON, L. M. 1972 *Theoretical Hydrodynamics.* Macmillan.

MORAWETZ, C. 1956 On the non-existence of continuous transonic flows past profiles. Part 1. *Comm. Pure Appl. Math.* **9**, 45–68.

MORAWETZ, C. 1957 On the non-existence of continuous transonic flows past profiles. Part 2. *Comm. Pure Appl. Math.* **10**, 107–131.

MURMAN, E. M. & COLE, J. D. 1971 Calculation of plane steady transonic flows. *A.I.A.A. J.* **9**, 114–121.

NIEUWLAND, G. Y. 1967 Transonic potential flow around a family of quasi-elliptical aerofoil sections. *Nat. Aerospace Lab., Amsterdam, Rep.* NRL TR T-172.

POWELL, M. J. D. 1964 A method for minimizing a sum of squares of nonlinear functions without calculating derivatives. *Computer J.* **7**, 303–307.

STEGER, J. L. & LOMAX, H. 1972 Transonic flow about two-dimensional airfoils by relaxation procedures. *A.I.A.A. J.* **10**, 49–54.

TAI, T. C. 1974 Transonic inviscid flow over lifting airfoils by the method of integral relations. *A.I.A.A. J.* **12**, 798–804.